How to cite: *Angew. Chem. Int. Ed.* **2022,** *61,* e202209464
International Edition: doi.org/10.1002/anie.202209464
German Edition: doi.org/10.1002/ange.202209464

Solar Cells

# Multidentate Chelation Heals Structural Imperfections for Minimized Recombination Loss in Lead-Free Perovskite Solar Cells

*Gengling Liu, Yang Zhong, Wenhuai Feng, Meifang Yang, Guo Yang, Jun-Xing Zhong, Tian Tian, Jian-Bin Luo, Junlei Tao, Shaopeng Yang, Xu-Dong Wang, Licheng Tan, Yiwang Chen,* and Wu-Qiang Wu**

**Abstract:** Tin-based perovskite solar cells (Sn-PSCs) have emerged as promising environmentally viable photovoltaic technologies, but still suffer from severe non-radiative recombination loss due to the presence of abundant deep-level defects in the perovskite film and under-optimized carrier dynamics throughout the device. Herein, we healed the structural imperfections of Sn perovskites in an "inside-out" manner by incorporating a new class of biocompatible chelating agent with multidentate claws, namely, 2-Guanidinoacetic acid (GAA), which passivated a variety of deep-level Sn-related and I-related defects, cooperatively reinforced the passivation efficacy, released the lattice strain, improved the structural toughness, and promoted the carrier transport of Sn perovskites. Encouragingly, an efficiency of 13.7 % with a small voltage deficit of ≈0.47 V has been achieved for the GAA-modified Sn-PSCs. GAA modification also extended the lifespan of Sn-PSCs over 1200 hours.

## Introduction

Metal halide perovskite solar cells (PSCs) have emerged as one of the most promising photovoltaic (PV) technologies due to their high-efficiency, low-cost and ease of solution processability.[1–3] Just within a short period of time, the power conversion efficiencies (PCEs) of PSCs have been elevated from 3.8 % to a certified value of 25.7 %.[4] More and more interest from both academic and industrial communities has been aroused, aiming to revolutionize the pathway towards more affordable electricity and new-generation PV products. However, the state-of-the-art, high-performing PSCs all contain toxic lead (Pb), which is unfriendly to the environment and human health, thus limiting the practical application of perovskite PVs.[5–7] To address this issue, a great deal of research efforts have been made on exploring some Pb-free analogues, such as antimony (Sb)-based, bismuth (Bi)-based, germanium (Ge)-based and tin (Sn)-based perovskites.[8–12] Among them, Sn-based perovskites have been regarded as one of the most prospective non-toxic light absorber candidates due to their prominent electronic structures and optoelectronic properties, which showcased great potential to approach the Shockley–Queisser limit of single junction solar cells.[13,14] Until now, the PCEs of Sn-based PSCs (Sn-PSCs) have been lifted to exceed 14 %, by means of composition tailoring,[15,16] interface modification,[17,18] additive engineering,[19–21] and processing optimization.[22–25] However, one could notice most of the state-of-the-art Sn-PSCs still suffered from unsatisfying photovoltage ($V_{oc}$, normally $<0.9$ V) and fill factor (*FF*, normally $<0.72$), which largely limited the further enhancement of device performance.

Sn perovskite is notorious for its uncontrolled crystallization kinetics and easy oxidation from $Sn^{2+}$ to $Sn^{4+}$, which results in the formation of low-quality Sn perovskite films with undesirable lattice distortion and abundant structural imperfections.[26–29] In general, there are several types of defects commonly found in Sn-based perovskites, including vacancies (i.e. $V_{Sn}$ and $V_I$), interstitials (i.e. $Sn_i$ and $I_i$) and antisite occupations (i.e. $Sn_I$ and $I_{Sn}$).[30] The previously reported strategies mainly focused on suppressing the formation of Sn vacancies ($V_{Sn}$) at the grain boundaries and/or on the film surface via employing passivation molecules (i.e. ammonium thiocyanate ($NH_4SCN$), acetic acid (HAc) or ethylenediammonium diiodide ($EDAI_2$), etc) or reducing agents (i.e. $SnF_2$, 4-acetamidophenol (AP), hydroquinone sulfonic acid (KHQSA) or Sn powder, etc).[19,31–37] In addition to $V_{Sn}$, other types of deep-level traps such as $Sn_I$ antisite and $I_{Sn}$ antisite, which easily formed within the internal lattice, are also the dominant non-radiative recombination centers in Sn-based perovskite films.[38] However, the significance of simultaneously passivating all of these

[*] G. Liu, W. Feng, M. Yang, G. Yang, Dr. J.-X. Zhong, Dr. T. Tian, J.-B. Luo, Prof. X.-D. Wang, Prof. W.-Q. Wu
Key Laboratory of Bioinorganic and Synthetic Chemistry (MoE), Lehn Institute of Functional Materials, School of Chemistry, Sun Yat-sen University
Guangzhou 510006 (China)
E-mail: wuwq36@mail.sysu.edu.cn

Y. Zhong, Prof. L. Tan, Prof. Y. Chen
Institute of Polymers and Energy Chemistry (IPEC), Nanchang University
999 Xuefu Avenue, Nanchang 330031 (China)
E-mail: ywchen@ncu.edu.cn

J. Tao, Prof. S. Yang
Province-Ministry Co-construction Collaborative Innovation Center of Hebei Photovoltaic Technology, College of Physics Science and Technology, Hebei University
Baoding 071002 (China)

detrimental point defects seems to be neglected. Lowering the dimensionality by constructing two dimension/three dimension (2D/3D) heterojunctions is another way to stabilize the Sn perovskites and improve $V_{oc}$. But it often came at a cost of sacrificing photocurrent density ($J_{sc}$) and *FF* owing to the uncontrolled phase distribution and crystal orientation of 2D components, which is adverse to charge transfer throughout the perovskite film thickness.[17,22] Therefore, it is highly desirable to explore a feasible approach that could concurrently passivate multiple types of deep-level defects and optimize the carrier dynamics, thus largely minimizing non-radiative recombination loss and achieving high-voltage Sn-PSCs with minimal voltage deficit.

In this work, we reported an intriguing inside-out healing strategy that could thoroughly heal the structural imperfections from the internal bulk to the surface of Sn perovskite films, which effectively passivates multiple intrinsic deep-level defects, especially the commonly neglected $Sn_I$ antisite, $I_{Sn}$ antisite, via introducing a biocompatible, multidentate chelator, namely, 2-Guanidinoacetic acid (GAA). We identified the synergic roles of amino and carbonyl functional groups in modulating crystallization kinetics, mitigating lattice distortion and manipulating carrier transport dynamics of Sn perovskite films and devices. Capitalized on these multifaceted advantages, the GAA-modified Sn-PSCs achieved a champion PCE of 13.70 %, and yielded an inspiring $V_{oc}$ of 0.93 V and a *FF* as high as 0.75. The target device showed remarkable long-term stability, which maintained nearly 93 % of its initial PCE after 1200 hours storage in inert gas atmosphere.

## Results and Discussion

It is well-known that the presence of multiple types of defects in solution-processed polycrystalline perovskite films will incur undesirable non-radiative recombination, which is detrimental to the device performance.[39] We firstly identified several types of intrinsic Sn-related and I-related defects (i.e. $V_{Sn}$, $V_I$, $Sn_I$ antisite ($V_I$ is occupied by Sn) and $I_{Sn}$ antisite defects ($V_{Sn}$ is occupied by I)) with different formation energies in Sn-based perovskites via density functional theory (DFT) calculations.[40] The calculated defect formation energies (DFEs) of $V_{Sn}$, $V_I$, $Sn_I$ and $I_{Sn}$ are 5.27 eV, 3.64 eV, −1.32 eV and 3.51 eV, respectively (Figure 1a). Specifically, the DFE of $Sn_I$ antisite defects is among the lowest value in these four types of defects, suggesting the dominant proportion of $Sn_I$ antisite defects in the whole defect profile of Sn perovskites, and effective passivation of them is imperative. Inspired by the functions of biocompatible GAA molecules in well-shaping the body muscles and facilitating their energy metabolism,[41] we expected the GAA molecules are capable of improving the structural toughness of Sn perovskites and reinforcing their capacity for more efficient solar energy conversion. GAA, a kind of multidentate chelator, possesses an ideal molecular configuration that contains a variety of functional groups, including carbonyl (C=O) and multiple amino groups (Figure S1), which is able to strengthen the passivation efficacy via forming coordination bonds and establishing hydrogen interaction with multiple species in Sn perovskites.[7] GAA incorporation and modification to a different extent increased the DFEs of $V_{Sn}$, $V_I$, $Sn_I$, and $I_{Sn}$ to 5.59 eV, 3.79 eV, −0.92 eV and 4.21 eV, respectively (Figure 1b, Figure S2), indicating the universal passivation effect of GAA on multiple types of Sn-related and I-related defects in target Sn perovskite film, especially for the $Sn_I$ and $I_{Sn}$ antisite defects. It should be noted that the interaction between different function groups or between polyatomic ions in one molecular additive/ingredient (i.e. multidentate molecules or polyatomic pseudo halides, etc) should be carefully tailored, which plays a critical role in affecting the defect passivation efficacy and longevity.[42,43] We then further analyzed and schematically illustrated the interaction mode and mechanism between different functional groups of GAA and Sn perovskite (Figure 1c). The Lewis base-typed "electron-donating" -$NH_2$ and C=O groups in GAA could both form coordination bonds with undercoordinated $Sn^{2+}$ ions in perovskites. Specifically, the -$NH_2$ group showcased a larger interaction energy to the Sn perovskite than that of C=O counterpart (i.e. −0.87 eV vs. −0.34 eV, Figure S3).[44] In addition, the C=O group could interact with antisite Sn, while the neighboring N–H could also interact with the $I^-$ of $SnI_6^{4-}$ octahedron through hydrogen bonding.[45] These favorable chemical interactions between GAA molecules and Sn perovskites can be experimentally confirmed by the peak shift of Sn 3d and I 3d signals in X-ray photoelectron spectroscopy (XPS) spectra (Figure S4). It is reported that the lone electron pair outside of the –$NH_2$ and C=O groups could localize the electron density around $Sn^{2+}$ for retarding its oxidation.[36] In our case, the GAA passivation dramatically reduced the $Sn^{4+}$ content of film surface from 15.9 % to 9.2 % (Figure 1d), which suggested the excellent antioxidation capability of GAA molecules, thus remarkably suppressing the formation of Sn vacancies in the resultant perovskite film. We also revealed that the antioxidation effect of GAA could be implemented throughout the whole perovskite film, namely, from top surface to internal bulk. This is confirmed by the depth-profiling XPS test, which consistently showed much smaller $Sn^{4+}/Sn^{2+}$ ratio in the GAA-modified perovskite film (Figure S5 and S6). The GAA incorporation also has a positive effect on improving the air stability of the as-prepared Sn perovskite precursor solutions. Upon intentional exposure in ambient air, the control perovskite ink quickly turned into dark red color owing to the rapid $Sn^{2+}$ oxidation, while the GAA-incorporated perovskite ink remained the same color after 15 min (Figure S7), reaffirming the antioxidation capability of GAA molecules even in the solvent medium. It is deduced that the GAA could strongly interact with the $Sn^{2+}$ species in the Sn perovskite precursor, which effectively retard the oxidation of $Sn^{2+}$ ions. The time-of-flight secondary ion mass spectroscopy (ToF-SIMS) tests further confirmed the molecular distribution of GAA throughout the perovskite film thickness, especially in the bulk region (Figure S8), which is consistent with the result from the XPS depth profile and indicates the great promise of GAA modification and passivation of Sn perovskite films via an

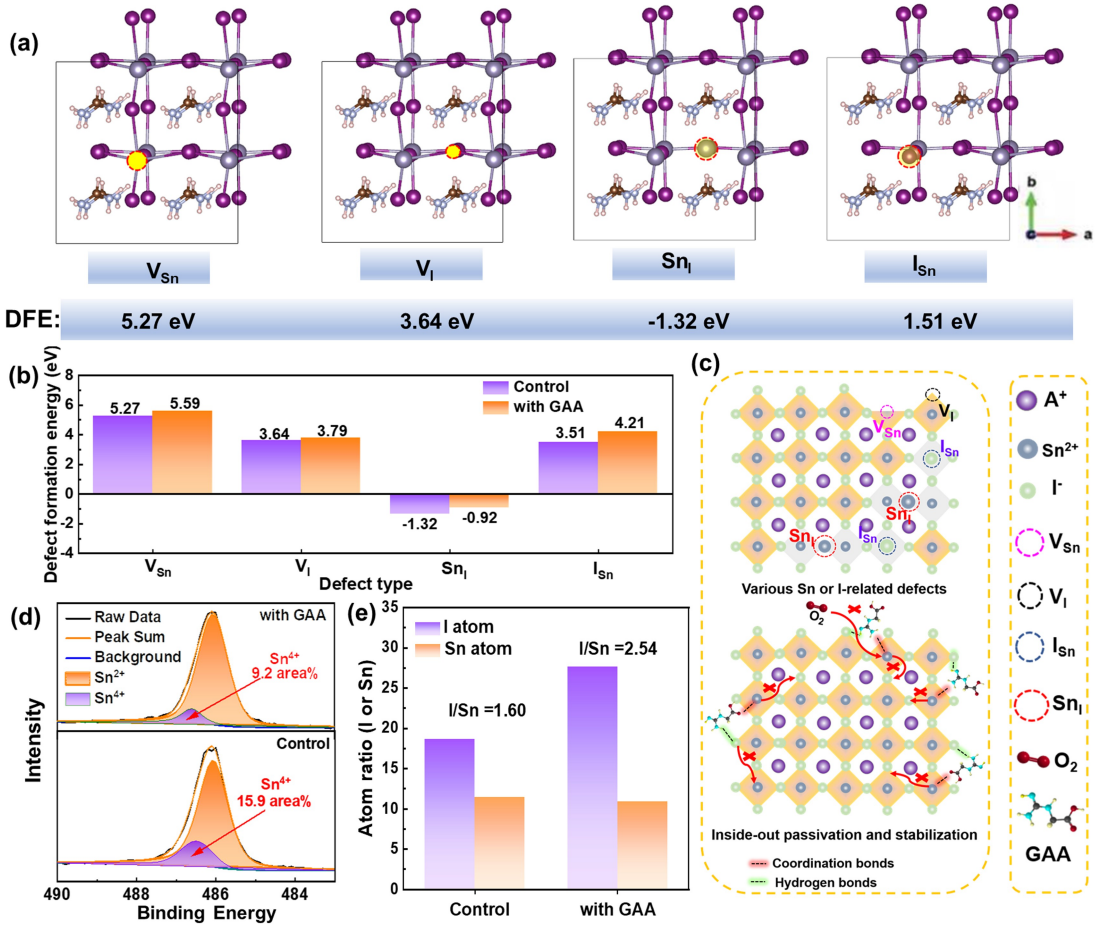


***Figure 1.*** a) Illustration of the crystallographic defects including $V_{Sn}$, $V_I$, $Sn_I$, $I_{Sn}$, and their corresponding DFEs. b) The comparison of DFEs of different defects for control and GAA-modified Sn perovskite. c) Schematic illustration of defect profile in pristine Sn perovskite film with a variety of Sn or I-related defects, and the inside-out passivation and stabilization of Sn perovskite via GAA interaction and modification. d) XPS spectra of Sn 3d and e) the atomic ratio of I/Sn for the control and GAA-modified Sn perovskite films.

intriguing inside-out manner. The Sn-based perovskites often exhibited severe self p-doping characteristic due to the presence of high $Sn^{4+}$ contents, which would to some extent unbalance the carrier transport and collection, thus aggregating the charge recombination.[46] We found that the GAA modification is able to de-dope the pristine Sn perovskite film and make it to be more n-type, as is evidenced by higher surface potential (Figure S9). This result again confirmed the antioxidation function of GAA molecules and their capability of mitigating the self p-doping effect. Distinguished to other reported additives with large molecular size that mainly stabilized the $Sn^{2+}$ and reduced the Sn vacancies on the perovskite film surface, the GAA with appropriate molecular size is expected to be also fit into the internal lattice and regulate the crystallization process for suppressing the formation of both Sn- and I-related antisite defects. The robust chemical interaction between GAA and perovskites also helped to reduce the halide deficiency. Specifically, the GAA-modified perovskite film maintained a higher I/Sn atomic ratio (2.54:1), which is closer to that of theoretically stoichiometric value (2.85:1) of our employed 2D/3D Sn perovskites ($PEA_{0.15}FA_{0.85}SnI_{2.85}Br_{0.15}$). In contrast, the control sample showed a considerable halide deficiency with a low I/Sn atomic ratio of only 1.60:1 (Figure 1e). The remarkably reduced halide deficiency of GAA-modified perovskite film can be mainly attributed to the effective suppression of I-related antisite defects, rather than the I-related vacancies. This indicated the halide deficiency in Sn perovskite is not mainly come from the escape of halide ions under thermal stress, since the annealing treatment is only conducted at 80 °C for 10 min. Instead, one should pay particular attention to normalize the coordination between metal ions and halide ions, which is conducive to suppress the formation of the Sn-related and I-related antisite defects, reduce the halide deficiency and stabilize the lattice of Sn perovskites. Overall, the cooperative multisite interaction and synergistic passivation effect induced by the multidentate functional groups in GAA with an optimal molecule configuration could thoroughly heal the structural imperfections in Sn perovskites and remarkably enhance the passivation efficacy, which is beneficial to improve the device performance of Sn-PSCs.

Subsequently, we further investigated the effect of GAA modification on the crystal structure, crystallinity and morphology of Sn perovskite films. The X-ray diffraction (XRD) results revealed that, relative to the control sample, the GAA incorporation remarkably improved the crystallinity of the perovskite film and facilitated its crystal growth along the (h00) orientation (Figure S10). Interestingly, one can notice that there is a XRD signal shown at a $2\theta$ degree of 5.4° for the control perovskite film, possibly corresponding to the formation of 2D $PEA_2SnI_4$ ($n=1$). In contrast, this signal disappeared and another XRD peak showed up at a $2\theta$ degree of 3.9°, which could be indexed as quasi-2D perovskites (i.e. $PEA_2FASn_2I_7$) with higher n values, namely, $n=2$ (Figure 2a). This result suggested the incorporated GAA molecules are able to modulate the crystallization kinetics, regulate the phase distribution and optimize the crystal orientation of 2D/3D structured Sn perovskites, especially tuning the quantum-well structure of low-dimensional perovskite components, thus affecting the carrier transport dynamics.[24,47] We implemented grazing-incidence wide-angle X-ray scattering (GIWAXS) technique to further verify the effect of GAA on modulating crystallization behavior of Sn-based perovskites. As illustrated in Figure 2b and c, the GIWAXS pattern of the control perovskite film exhibited some dispersive Debye–Scherrer rings corresponding to (100) and (200) crystal planes.[48] In contrast, the GAA-modified perovskite film showed concentrated Bragg spots with reinforced intensity at similar positions, which further confirmed the preferential crystal growth of perovskite along the {$h$00} orientation. Introducing a small amount (i.e. 0.01 mM) of GAA slightly improved the light absorption capability of resultant perovskite film owing to its improved quality (Figure S11). The top-view and cross-sectional scanning electron microscopy (SEM) images of the perovskite films with or without GAA modification have been investigated. The control perovskite film presented abundant randomly distributed pin-holes, while the GAA-modified perovskite film exhibited a relatively dense morphology with reduced pin-holes (Figure S12). Note, the Sn perovskite film modified with moderate concentration of GAA (i.e. 0.01 mM) showcased the optimal film quality with both high crystallinity and good surface coverage. Moreover, the GAA-perovskite film exhibited distinctly ordered distribution of crystals, whereas the control perovskite film presented multilayered crystals with random orientation (Figure 2d and e). All these results revealed that GAA played positive roles on the crystallization modulation and defect management of Sn perovskite, which could effectively

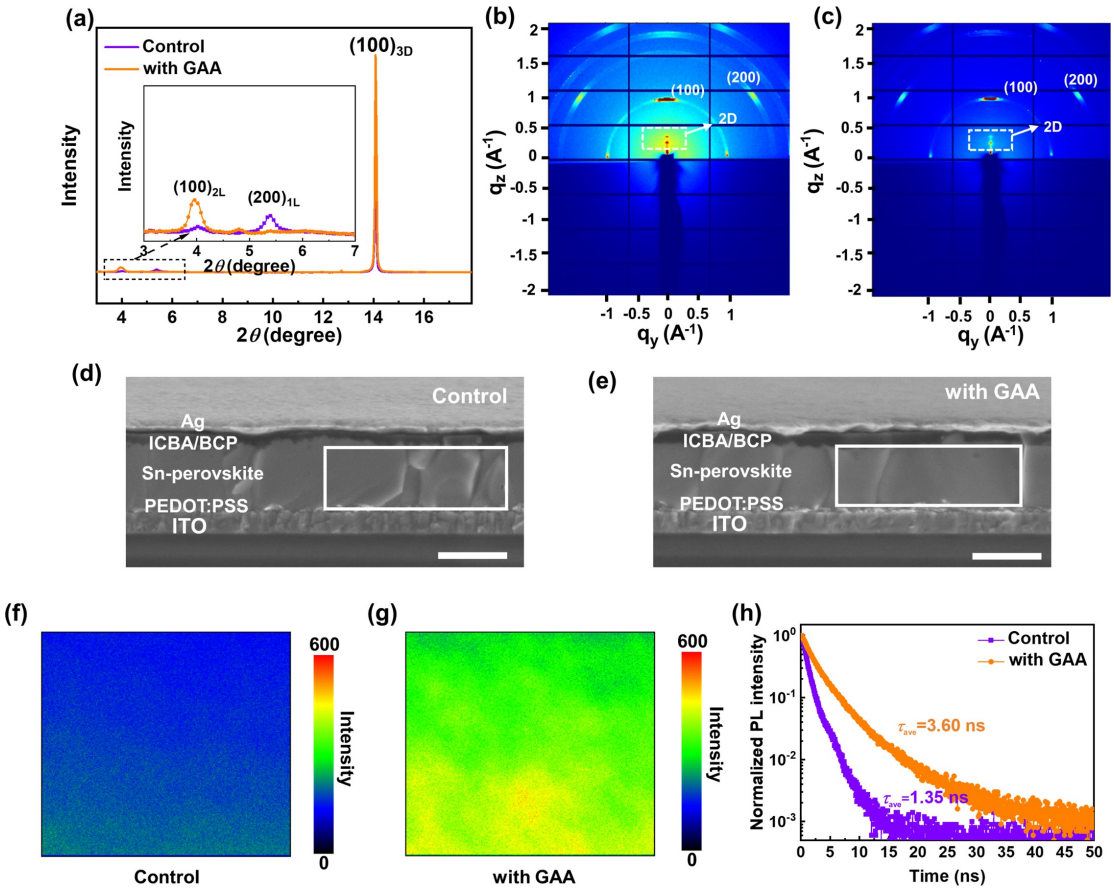


***Figure 2.*** a) XRD patterns of the control and GAA-modified Sn perovskite films. GIWAXS patterns of b) control and c) GAA-modified Sn perovskite films. Cross-sectional SEM images of d) control and e) GAA-modified Sn perovskite devices. PL mappings of f) control and g) GAA-modified perovskite films deposited on glass substrates. h) TRPL decay of control and GAA-modified Sn perovskite films.

inhibit non-radiative recombination and facilitate carrier transport within the perovskite films and corresponding devices, as will be discussed latter.

To better understand the beneficial roles of GAA modification on improving the optoelectronic properties of Sn perovskite films, we carried out a series of optical characterizations for the control and GAA-modified perovskite films. Specifically, the confocal photoluminescence (PL) mapping images showed a stronger PL intensity in GAA-modified perovskite film, relative to that of the control film (Figure 2f and g). Similar trend has been observed in steady-state PL intensity spectra, with the 0.01 mM GAA-modified perovskite film exhibiting the strongest PL intensity (Figure S13). Besides, the time-resolved PL (TRPL) decay characterizations showed a prolonged PL lifetime of 3.60 ns for the GAA-modified perovskite film (Figure 2h), which is approximately 3-folds longer than that of the control perovskite film (1.35 ns, Figure 2h and Table S1). The enhanced PL intensity and extended PL lifetime can be ascribed to abovementioned improved quality of perovskite film with GAA modification and passivation.

It is well-known that the residual tensile strain ($\sigma$) is easily formed during the crystallization process of perovskite films, which plays a key role in affecting the device performance, especially the stability of PSCs.[32] Just like strengthening the muscles of human beings via the assist of biocompatible GAA molecules, we expect the GAA additives could also be capable of manipulating the residual strain of the perovskite films at a macroscopic level. We thus analyzed the residual strain of the Sn perovskite films using grazing incidence x-ray diffraction (GIXRD) characterizations. The GIXRD peak of the control perovskite film steadily shifted to a lower angle as the instrumental tilt angle ($\Psi$) goes from 0° to 20°, and the corresponding fitted $2\theta$-Sin$^2(\Psi)$ line displayed a steep slope, suggesting the presence of considerable tensile strain within the crystal lattice of perovskite, thus causing severe lattice distortion (Figure 3a).[49] Surprisingly, the residual strain has been substantially released in the GAA-modified perovskite film, as is evidenced by mitigated GIXRD peak shift and flatten slope of corresponding $2\theta$-Sin$^2(\Psi)$ curve (Figure 3b, c and d). To better understand the GAA-assisted strain regulation mechanism at an atomic scale, we calculated the Sn–I spacing in perovskite lattice with or without GAA interaction and modification. As a result, the Sn–I spacing of perovskite lattice decreased from 3.12 Å to 3.02 Å upon GAA anchoring, a hint of inhibited lattice expansion and thus mitigated lattice distortion (Figure 3e).

To gain deep insights into the ultrafast photo-excited carrier transfer dynamics at the relevant interfaces within the devices at a timescale of picoseconds, we further conducted the femtosecond transient absorption spectroscopy (fs-TA) measurements for the multilayer stack with the perovskite film sandwiched between PEDOT:PSS and ICBA (Figure 4a). The contour plots of the TA spectra for both the control and GAA-modified samples showed two distinct ground-state bleaching (GSB) peaks at ≈640 nm and ≈770 nm, which corresponded to the transient bleaching of 2D and 3D perovskites, respectively.[33] In general, the intensity of GSB reflects the photo-induced carrier population in the conduction and valance bands of perovskite, and hence the charge transfer dynamics from perovskite to adjacent contact carrier transport layer can be monitored visually by observing the quenching rates of GSB signal. As compared to the control sample, a more promptly faded GSB signal has been observed in the contour plot of the GAA-modified sample (Figure 4b and c), suggesting more efficient extraction of the photogenerated electrons from GAA-modified perovskite layer to the adjacent carrier

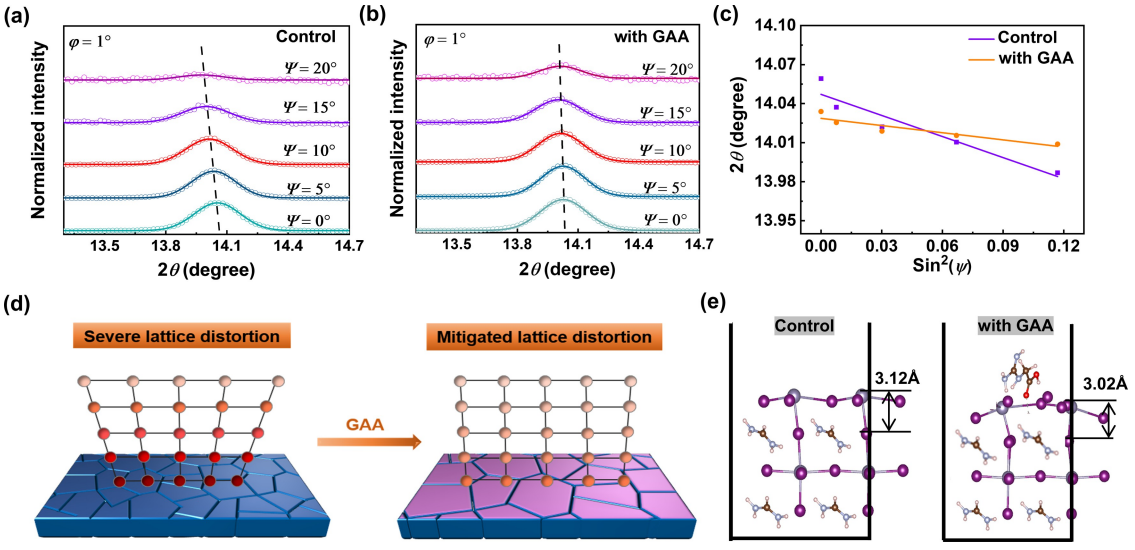


***Figure 3.*** The GIXRD diffraction peaks in the condition of $\phi = 1°$ shift as instrumental $\Psi$ values goes from 0° to 20° for (a) control and b) GAA-modified perovskite films. c) Linear fit of 2θ–Sin$^2(\Psi)$ of the corresponding perovskite films. d) Schematic of the tensile strain and lattice distortion conditions for the Sn perovskite before and after GAA modification. e) DFT calculations of Sn–I spacing in Sn perovskite lattice with or without GAA anchoring.

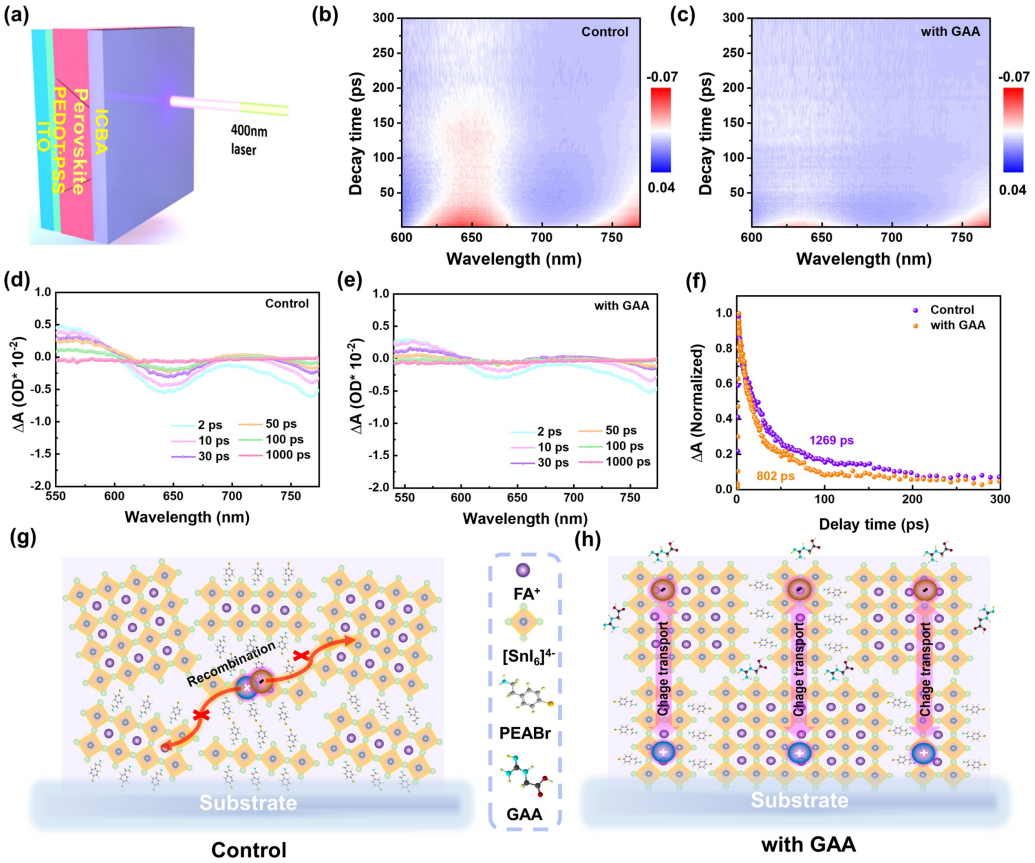


***Figure 4.*** a) Schematic of the multilayer stacks (ITO/PEDOT:PSS/Perovskite/ICBA) for the TA measurement, where a 400 nm pump pulse generated by a fs-laser was used to probe the TA signal. The contour plot and delay time-dependent TA spectra of (b), (d) control device and (c), (e) GAA-modified device. f) Dynamic TA decay of 3D perovskite phase probed at the GSB peak of ≈769 nm for the control and GAA-modified perovskite devices. Sketch showing the charge transport and recombination behavior in g) control and h) GAA-modified perovskite films.

transport layers.[50,51] The GSB peak intensity at the same delay time of the GAA-modified sample appeared to be much weaker, relative to the control counterpart (Figure 4d and e), which is in good agreement with the results of contour plots of the TA spectra. The GSB decay kinetics have been further interpreted by three exponential fitting to understand the charge transfer and carrier recombination dynamics. First, we individually analyzed the GSB decay kinetics of 2D or 3D perovskite components, and the fitted decay lifetimes have been summarized in Table S2. Several previous works have demonstrated the favorable energy transfer from 2D to 3D perovskite phase, and the 3D phase is primarily responsible for transporting the collected and/or photo-generated carriers to the adjacent contacts.[52–54] In our case, the decay lifetime of the 2D phase in GAA-modified sample is almost 2-fold faster than that of the control sample (5509.6 ps vs. 11346.2 ps, Figure S14), suggesting more efficient energy transfer to 3D components. This can be attributed to the precise control of the layer number distribution (i.e. obtaining higher n values) and rational modulation of crystal orientation in 2D perovskite structures with the assist of GAA modification, which strongly weakened the quantum hydrazine domain-limiting effect and facilitated the charge transfer in 2D/3D perovskite. In terms of the 3D perovskite phase, the carrier dynamics can be interpreted to three processes. Specifically, $\tau_1$ reflected the charge transfer process from 3D perovskite to adjacent contacts, $\tau_2$ was related to the energy received from the 2D perovskite phase, and $\tau_3$ could be correlated to the process of trap-assisted carrier recombination within perovskite.[55] As a result, one could observe the remarkable decrease of $\tau_1$ and increase of both $\tau_2$ and $\tau_3$ for GAA-modified sample (Table S2), indicating the GAA modification could ensure efficient energy transfer from 2D phase to 3D components, boost the charge extraction and collection to adjacent carrier transport layers, as well as prolong the carrier recombination lifetime in target 2D/3D Sn perovskite structures. Overall, the GAA-modified sample showcased accelerated charge transfer rate than that of the control sample, regardless of 2D or 3D perovskite components (i.e. 801.9–5509.6 ps vs. 1269.4–11346.2 ps) (Figure 4f and Figure S14). All above results verified the beneficial roles of GAA-assisted chemical modification and passivation on accelerating carrier extraction and collection through well-integrated 2D/3D Sn perovskites with improved crystallinity and preferable orientation, well-controlled phase distribution, optimized quantum-well structures and favorable energy transfer, released lattice strain, as well as universal

defect passivation, thereby enormously minimizing the non-radiative recombination loss. In contrast, the control Sn perovskite sample exhibits disordered crystal orientation and uncontrolled phase distribution, which would induce unfavorable recombination pathways and incur severe non-radiative recombination loss (Figure 4g and h).

We fabricated the Sn-PSCs with the device architectures of indium-doped tin oxide (ITO)/PEDOT:PSS/Sn perovskite (with or w/o GAA)/ICBA/bathocuproine (BCP)/Ag (Figure 5a). The current density-voltage ($J$–$V$) curves of the PSCs based on the control and GAA-modified perovskite films were displayed in Figure 5b, and the corresponding photovoltaic parameters were summarized in Table 1. The control device exhibited a champion PCE of 9.34 %, accompanied by an open-circuit voltage ($V_{oc}$) of 0.83 V, a short-circuit current ($J_{sc}$) of 17.08 mA cm$^{-2}$ and a fill factor ($FF$) of 65.7 %, as well as a severe hysteresis. Encouragingly, incorporating a trace amount of GAA additives to the perovskite ink is able to improve all the photovoltaic parameters and overall device performances. Typically, the optimal concentration of GAA was determined to be 0.01 mM (Figure S15 and Table S3), which enabled to deliver a champion PCE of 13.70 % with a negligible $J$–$V$ hysteresis, accompanied by a $V_{oc}$ of 0.93 V, a $J_{sc}$ of

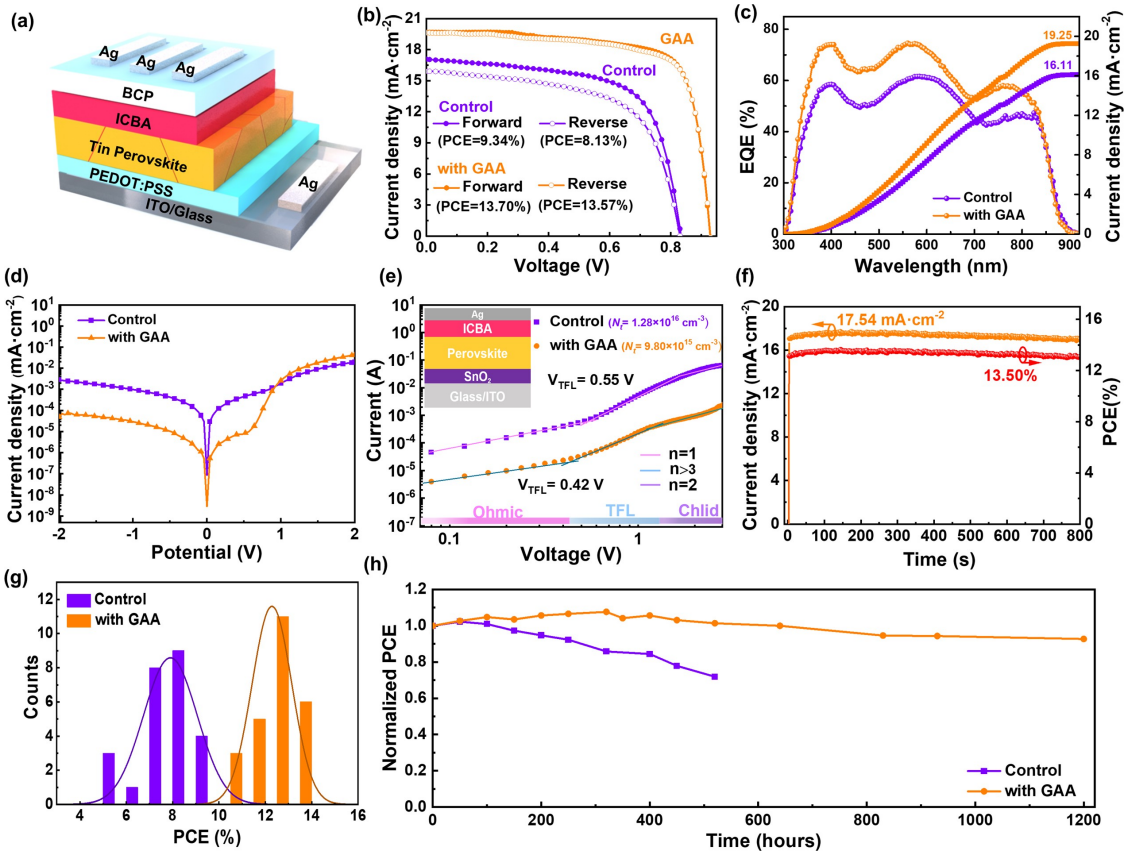


***Figure 5.*** a) Schematic illustration of the device architecture of Sn-PSC. b) $J$–$V$ curves of the Sn-PSCs without or with GAA modification. c) EQE spectra and integrated $J_{sc}$ values of the Sn-PSCs with or without GAA modification. d) Dark $J$–$V$ curves of the PSCs with or without GAA modification. e) SCLC measurement of the trap-state density for the control and GAA-modified perovskite films. Inset shows the architecture of electron-only devices. f) Stabilized current density and PCE of the GAA-modified Sn-PSCs operated at the maximum power point of 0.77 V. g) PCE distribution histogram of 25 devices without or with GAA modification. h) Trace of long-term stability for Sn-PSCs without or with GAA modification upon storage in inert gas environment.

***Table 1:*** Summarized photovoltaic parameters of the Sn-PSCs with or without GAA modification under AM 1.5G one sun irradiation (100 mW cm$^{-2}$).

| PSCs | Scan direction | $V_{oc}$ [V] | $J_{sc}$ [mA cm$^{-2}$] | FF [%] | PCE [%] | Average PCE [%] |
|---|---|---|---|---|---|---|
| Control | Forward | 0.83 | 17.08 | 65.7 | 9.34 | 7.90 ± 1.14 |
| | Reverse | 0.83 | 15.92 | 61.6 | 8.13 | |
| with GAA | Forward | 0.93 | 19.66 | 74.9 | 13.70 | 12.29 ± 0.84 |
| | Reverse | 0.93 | 19.62 | 74.4 | 13.57 | |

Note: the average PCE is determined by at least 25 devices for each condition.

19.66 mA cm$^{-2}$ and a FF of 74.9 %, which is ≈47 % higher than that of the control device. Obviously, the remarkable enhancement of overall device performance of Sn-PSCs with GAA modification can be attributed to the concurrent improvement of $J_{sc}$, $V_{oc}$ and FF. Specifically, the $J_{sc}$ and FF enhancement can be mainly ascribed to the facilitated carrier extraction and collection owing to the improved quality of GAA-modified Sn perovskite film with improved crystallinity, favorable crystal orientation, as well as balanced carrier separation and transport.

The external quantum efficiency (EQE) spectra were measured to check the reliability of the enhanced photocurrent. As compared to the control counterpart, the GAA-modified Sn-PSCs exhibited higher EQE values over the wavelength region from 350 nm to 850 nm, corresponding to higher integrated current density (i.e. 19.25 mA cm$^{-2}$ vs. 16.11 mA cm$^{-2}$, Figure 5c), which is in good accordance with the $J_{sc}$ obtained from the *J–V* curves. The GAA-modified device showcased a lower leakage current and more efficient carrier injection rate than that of the control device (Figure 5d), further verifying the reduced shunting paths and facilitated charge extraction benefited from the better morphology of perovskite film with improved surface coverage and optoelectronic properties.[55] We attributed the considerable enhancement of $V_{oc}$ by ≈100 mV to the effective passivation of multiple types of deep-level defects in an universal manner and inhibition of $Sn^{2+}$ oxidation with the assist of biocompatible multidentate GAA chelators, which is beneficial to greatly reduce the non-radiative recombination and promote the device performance of resultant Sn-PSCs. We quantified the defect state density of the Sn perovskite film with or without GAA passivation by using the space charge limited current (SCLC) technique. The electron-only device featuring an architecture of ITO/$SnO_2$/Sn perovskite (with or w/o GAA)/ICBA/Ag has been employed in SCLC measurement (inset in Figure 5e). As a result, the $V_{TFL}$ (onset voltage of trap-filled limit region) and trap density ($N_t$) can be determined and calculated using the following Equation (1):[56]

$$N_t = \frac{2\varepsilon_0\varepsilon_r V_{TFL}}{qL^2} \quad (1)$$

where $L$, $\varepsilon_0$ and $\varepsilon$ denote the thickness (≈250 nm), vacuum permittivity and dielectric constant of the perovskite film, respectively. Specifically, the GAA-modified device showed a smaller $V_{TFL}$ of 0.42 V than that of the control device (0.55 V). The $N_t$ values of GAA-passivated device ($9.80\times10^{15}$ cm$^{-3}$) is approximately one fourth lower than that of the control counterpart ($1.28\times10^{16}$ cm$^{-3}$) (Figure 5e).

The best-performing device showed a stabilized PCE of 13.50 % for 800 s measured at a maximum-power-point of 0.77 V (Figure 5f). In addition, the PCE histogram of the Sn-PSCs with or without GAA modification was presented in Figure 5g, in which the data was collected from a batch of 25 devices for each condition. Specifically, the GAA-modified devices demonstrated a narrower PCE distribution with nearly 70 % of devices yielding PCEs above 13 %. This result highlighted the effectiveness of GAA modification and passivation on improving the device performance and ensuring better reproducibility for the lead-free, environmentally viable perovskite photovoltaics.

The long-term stability of Sn-PSCs is also a critical evaluation criterion for accessing their suitability towards practical application and commercialization.[57] We traced the evolution of PCEs over time for the unencapsulated control and GAA-modified Sn-PSCs upon storage in $N_2$ atmosphere. As demonstrated in Figure 5h, there is an opposite behavior of PCE evolution for the control and GAA-modified PSCs at the first 300 hours. The PCE degradation in control device could be attributed to the easy oxidation and decomposition of Sn perovskites, especially when the *J–V* measurement of unencapsulated device was conducted in ambient air, which would speed up the decline of PCE. During the same period, the GAA-modified PSC witnessed an increase of PCE, which can be attributed to the effective defect passivation and anti-oxidation function of GAA molecules. This result is exactly consistent with the previous reports showing that most of the well-passivated PSCs required certain durations of aging to realize grain coarsening, compositions homogenization and/or self-healing of perovskite films, thus maximizing the photovoltaic performances.[42,48] The GAA-modified device maintained 93 % of its initial efficiency after aging for 1200 hours, while the control device quickly degraded to 80 % of its original efficiency after 520 hours. We attributed the extended lifespan of GAA-modified device to the effective inside-out healing of structural imperfections, relaxation of lattice tensile strain and optimization of carrier dynamics.

## Conclusion

We identified that, rather than the commonly studied surface Sn vacancies, the presence of more easily formed Sn-related and I-related antisite defects in Sn perovskites dominated the non-radiative recombination loss in the resultant PSCs. We developed a novel inside-out structural-imperfections healing strategy by simply incorporating a trace amount of biocompatible GAA molecules with multidentate functional groups into Sn perovskites. The GAA could passivate multiple types of deep-level defects from the internal lattice to the crystal surface of the Sn perovskites, thus to a large extent, minimizing the defect-induced non-radiative recombination loss, and being more superior to other reported single-function additives and/or reduction agents.[30] GAA modification is also able to modulate the crystallization kinetics, mitigate the lattice distortion, regulate the phase distribution of 2D/3D perovskites and optimize the carrier transport dynamics, thus affording a superior device performance with a PCE of 13.70 % and an improved stability up to 1200 hours, accompanied by a high $V_{oc}$ of 930 mV, corresponding to a small voltage loss of 0.47 V. This work provides a new and in-depth insight to facilitate the understanding of the defect profile and differentiated formation tendency of various types of deep-level defects in Sn-based perovskite and highlights the significance of universal defect passivation for the fabrication of

highly efficient and stable lead-free, environmentally-friendly photovoltaic devices.

## Acknowledgements

The authors acknowledge the financial support from the National Key R&D Program of China (2019YFB1503200), the National Natural Science Foundation of China (22005355), National Natural Science Foundation of China (NSFC) (U20A20128), Guangdong Basic and Applied Basic Research Foundation (2022A1515010282) and the Fundamental Research Funds for the Central Universities, Sun Yat-sen University (22qntd2305).

## Conflict of Interest

The authors declare no conflict of interest.

## Data Availability Statement

The data that support the findings of this study are available from the corresponding author upon reasonable request.

**Keywords:** Defects · Perovskites · Solar Cells · Stability · Tin

[1] S. D. Stranks, G. E. Eperon, G. Grancini, C. Menelaou, M. J. Alcocer, T. Leijtens, L. M. Herz, A. Petrozza, H. J. Snaith, *Science* **2013**, *342*, 341–344.
[2] J.-F. Liao, W.-Q. Wu, Y. Jiang, J.-X. Zhong, L. Wang, D.-B. Kuang, *Chem. Soc. Rev.* **2020**, *49*, 354–381.
[3] Y. Tan, X. Chang, B.-X. Lei, W. Q. Wu, *J. Energy Chem.* **2022**, *66*, 525–528.
[4] NREL, National Renewable Energy Laboratory Best Research Cell Efficiency Chart, https://www.nrel.gov/pv/cell-efficiency.html (accessed: May 2022).
[5] C. Liu, J. Tu, X. Hu, Z. Huang, X. Meng, J. Yang, X. Duan, L. Tan, Z. Li, Y. Chen, *Adv. Funct. Mater.* **2019**, *29*, 1808059.
[6] Z. Li, P. Wang, C. Ma, F. Igbari, Y. Kang, K.-L. Wang, W. Song, C. Dong, Y. Li, J. Yao, D. Meng, Z.-K. Wang, Y. Yang, *J. Am. Chem. Soc.* **2021**, *143*, 2593–2600.
[7] Z. Liang, H. Xu, Y. Zhang, G. Liu, S. Chu, Y. Tao, X. Xu, S. Xu, L. Zhang, X. Chen, *Adv. Mater.* **2022**, *34*, 2110241.
[8] B. Vargas, E. Ramos, E. Pérez-Gutiérrez, J. C. Alonso, D. Solis-Ibarra, *J. Am. Chem. Soc.* **2017**, *139*, 9116–9119.
[9] G. Liu, C. Liu, Z. Lin, J. Yang, Z. Huang, L. Tan, Y. Chen, *ACS Appl. Mater. Interfaces* **2020**, *12*, 14049–14056.
[10] S. J. Lee, S. S. Shin, Y. C. Kim, D. Kim, T. K. Ahn, J. H. Noh, J. Seo, S. I. Seok, *J. Am. Chem. Soc.* **2016**, *138*, 3974–3977.
[11] B. W. Park, B. Philippe, X. Zhang, H. Rensmo, G. Boschloo, E. M. Johansson, *Adv. Mater.* **2015**, *27*, 6806–6813.
[12] F. Jiang, D. Yang, Y. Jiang, T. Liu, X. Zhao, Y. Ming, B. Luo, F. Qin, J. Fan, H. Han, *J. Am. Chem. Soc.* **2018**, *140*, 1019–1027.
[13] F. Hao, C. C. Stoumpos, D. H. Cao, R. P. Chang, M. G. Kanatzidis, *Nat. Photonics* **2014**, *8*, 489–494.
[14] M. H. Kumar, S. Dharani, W. L. Leong, P. P. Boix, R. R. Prabhakar, T. Baikie, C. Shi, H. Ding, R. Ramesh, M. Asta, M. Graetzel, S. Mhaisalkar, N. Mathews, *Adv. Mater.* **2014**, *26*, 7122–7127.
[15] B. B. Yu, Z. Chen, Y. Zhu, Y. Wang, B. Han, G. Chen, X. Zhang, Z. Du, Z. He, *Adv. Mater.* **2021**, *33*, 2102055.
[16] M. Li, W.-W. Zuo, Y.-G. Yang, M. Aldamasy, Q. Wang, S. H. T. Cruz, S.-L. Feng, M. Saliba, Z.-K. Wang, A. Abate, *ACS Energy Lett.* **2020**, *5*, 1923–1929.
[17] X. Jiang, F. Wang, Q. Wei, H. Li, Y. Shang, W. Zhou, C. Wang, P. Cheng, Q. Chen, L. Chen, Z. Ning, *Nat. Commun.* **2020**, *11*, 1245.
[18] J.-J. Cao, Y.-H. Lou, W.-F. Yang, K.-L. Wang, Z.-H. Su, J. Chen, C.-H. Chen, C. Dong, X.-Y. Gao, Z.-K. Wang, *Chem. Eng. J.* **2022**, *433*, 133832.
[19] Q. Tai, X. Guo, G. Tang, P. You, T. W. Ng, D. Shen, J. Cao, C. K. Liu, N. Wang, Y. Zhu, C.-s. Lee, F. Yan, *Angew. Chem. Int. Ed.* **2019**, *58*, 806–810; *Angew. Chem.* **2019**, *131*, 816–820.
[20] X. Liu, T. Wu, J.-Y. Chen, X. Meng, X. He, T. Noda, H. Chen, X. Yang, H. Segawa, Y. Wang, L. Han, *Energy Environ. Sci.* **2020**, *13*, 2896–2902.
[21] T.-B. Song, T. Yokoyama, C. C. Stoumpos, J. Logsdon, D. H. Cao, M. R. Wasielewski, S. Aramaki, M. G. Kanatzidis, *J. Am. Chem. Soc.* **2017**, *139*, 836–842.
[22] X. Jiang, H. Li, Q. Zhou, Q. Wei, M. Wei, L. Jiang, Z. Wang, Z. Peng, F. Wang, Z. Zang, K. Xu, Y. Hou, S. Teale, W. Zhou, R. Si, X. Gao, E. H. Sargent, Z. Ning, *J. Am. Chem. Soc.* **2021**, *143*, 10970–10976.
[23] T. Wang, H. L. Loi, J. Cao, Z. Qin, Z. Guan, Y. Xu, H. Cheng, M. G. Li, C. S. Lee, X. Lu, F. Yan, *Adv. Sci.* **2022**, *9*, 2200242.
[24] D. Cui, X. Liu, T. Wu, X. Lin, X. Luo, Y. Wu, H. Segawa, X. Yang, Y. Zhang, Y. Wang, L. Han, *Adv. Funct. Mater.* **2021**, *31*, 2100931.
[25] F. Li, C. Zhang, J. H. Huang, H. Fan, H. Wang, P. Wang, C. Zhan, C. M. Liu, X. Li, L. M. Yang, Y. Song, K.-J. Jiang, *Angew. Chem. Int. Ed.* **2019**, *58*, 6688–6692; *Angew. Chem.* **2019**, *131*, 6760–6764.
[26] B. Li, H. Di, B. Chang, R. Yin, L. Fu, Y. N. Zhang, L. Yin, *Adv. Funct. Mater.* **2021**, *31*, 2007447.
[27] M. Hu, R. Nie, H. Kim, J. Wu, S. Chen, B.-w. Park, G. Kim, H.-W. Kwon, S. I. Seok, *ACS Energy Lett.* **2021**, *6*, 3555–3562.
[28] E. L. Lim, A. Hagfeldt, D. Bi, *Energy Environ. Sci.* **2021**, *14*, 3256–3300.
[29] B. Chen, P. N. Rudd, S. Yang, Y. Yuan, J. Huang, *Chem. Soc. Rev.* **2019**, *48*, 3842–3867.
[30] B. Li, B. Chang, L. Pan, Z. Li, L. Fu, Z. He, L. Yin, *ACS Energy Lett.* **2020**, *5*, 3752–3772.
[31] F. Wang, X. Jiang, H. Chen, Y. Shang, H. Liu, J. Wei, W. Zhou, H. He, W. Liu, Z. Ning, *Joule* **2018**, *2*, 2732–2743.
[32] Y. Su, J. Yang, G. Liu, W. Sheng, J. Zhang, Y. Zhong, L. Tan, Y. Chen, *Adv. Funct. Mater.* **2022**, *32*, 2109631.
[33] Z. Zhu, C. C. Chueh, N. Li, C. Mao, A. K. Y. Jen, *Adv. Mater.* **2018**, *30*, 1703800.
[34] M. E. Kayesh, K. Matsuishi, R. Kaneko, S. Kazaoui, J.-J. Lee, T. Noda, A. Islam, *ACS Energy Lett.* **2019**, *4*, 278–284.
[35] X. Cao, J. Li, H. Dong, P. Li, Q. Fan, R. Xu, H. Li, G. Zhou, Z. Wu, *Adv. Funct. Mater.* **2021**, *31*, 2104344.
[36] E. Jokar, C.-H. Chien, A. Fathi, M. Rameez, Y.-H. Chang, E. W.-G. Diau, *Energy Environ. Sci.* **2018**, *11*, 2353–2362.
[37] F. Gu, S. Ye, Z. Zhao, H. Rao, Z. Liu, Z. Bian, C. Huang, *Sol. RRL* **2018**, *2*, 1800136.
[38] X. Jiang, Z. Zang, Y. Zhou, H. Li, Q. Wei, Z. Ning, *Acc. Mater. Res.* **2021**, *2*, 210–219.
[39] W. Shockley, W. Read Jr, *Phys. Rev.* **1952**, *87*, 835.
[40] X. Gu, W. Xiang, Q. Tian, S. F. Liu, *Angew. Chem. Int. Ed.* **2021**, *60*, 23164–23170; *Angew. Chem.* **2021**, *133*, 23348–23354.
[41] Y. Liu, J. Li, Y. Li, T. Gao, L. Zhang, F. Gao, G. Zhou, *Anim. Feed Sci. Technol.* **2015**, *205*, 82–89.
[42] E. Jokar, H.-S. Chuang, C.-H. Kuan, H.-P. Wu, C.-H. Hou, J. Shyue, E. W.-G. Diau, *J. Phys. Chem. Lett.* **2021**, *12*, 10106–10111.

[43] D. B. Khadka, Y. Shirai, M. Yanagida, K. Miyano, *ACS Appl. Energy Mater.* **2021**, *4*, 12819–12826.
[44] W.-Q. Wu, Z. Yang, P. N. Rudd, Y. Shao, X. Dai, H. Wei, J. Zhao, Y. Fang, Q. Wang, Y. Liu, Y. Deng, X. Xiao, Y. Feng, J. Huang, *Sci. Adv.* **2019**, *5*, eaav8925.
[45] R. Wang, J. Xue, K.-L. Wang, Z.-K. Wang, Y. Luo, D. Fenning, G. Xu, S. Nuryyeva, T. Huang, Y. Zhao, J. L. Yang, J. Zhu, M. Wang, S. Tan, I. Yanuz, K. N. Houk, Y. Yang, *Science* **2019**, *366*, 1509–1513.
[46] M. Pitaro, E. K. Tekelenburg, S. Shao, M. A. Loi, *Adv. Mater.* **2022**, *34*, 2105844.
[47] D. Yu, Q. Wei, H. Li, J. Xie, X. Jiang, T. Pan, H. Wang, M. Pan, W. Zhou, W. Liu, P. C. Y. Chow, Z. Ning, *Angew. Chem. Int. Ed.* **2022**, *61*, e202202346; *Angew. Chem.* **2022**, *134*, e202202346.
[48] C. Ran, W. Gao, J. Li, J. Xi, L. Li, J. Dai, Y. Yang, X. Gao, H. Dong, B. Jiao, I. Spanopoulos, C. D. Malliakas, X. Hou, M. G. Kanatzidis, Z. Wu, *Joule* **2019**, *3*, 3072–3087.
[49] L. Rao, X. Meng, S. Xiao, Z. Xing, Q. Fu, H. Wang, C. Gong, T. Hu, X. Hu, R. Guo, Y. Chen, *Angew. Chem. Int. Ed.* **2021**, *60*, 14693–14700; *Angew. Chem.* **2021**, *133*, 14814–14821.
[50] W. Q. Wu, J. F. Liao, J. X. Zhong, Y. F. Xu, L. Wang, J. Huang, *Angew. Chem. Int. Ed.* **2020**, *59*, 20980–20987; *Angew. Chem.* **2020**, *132*, 21166–21173.
[51] Y.-N. Lu, J.-X. Zhong, Y. Yu, X. Chen, C.-Y. Yao, C. Zhang, M. Yang, W. Feng, Y. Jiang, Y. Tan, L. Gong, X. Wei, Y. Zhou, L. Wang, W.-Q. Wu, *Energy Environ. Sci.* **2021**, *14*, 4048–4058.
[52] Z. Guo, Y. Zhang, B. Wang, L. Wang, N. Zhou, Z. Qiu, N. Li, Y. Chen, C. Zhu, H. Xie, T. Song, L. Song, H. Xue, S. Tao, Q. Chen, G. Xing, L. Xiao, Z. Lu, H. Zhou, *Adv. Mater.* **2021**, *33*, 2102246.
[53] L. Lei, D. Seyitliyev, S. Stuard, J. Mendes, Q. Dong, X. Fu, Y. A. Chen, S. He, X. Yi, L. Zhu, C.-H. Chang, H. Ade, K. Gundogdu, F. So, *Adv. Mater.* **2020**, *32*, 1906571.
[54] C. Liu, Y. Liu, S. Wang, J. Liang, C. Wang, F. Yao, W. Ke, Q. Lin, T. Wang, C. Tao, G. Fang, *Adv. Opt. Mater.* **2022**, *10*, 2200276.
[55] Z. Ren, J. Yu, Z. Qin, J. Wang, J. Sun, C. C. Chan, S. Ding, K. Wang, R. Chen, K. S. Wong, X. Lu, W.-J. Yin, W. C. Choy, *Adv. Mater.* **2021**, *33*, 2005570.
[56] G. Liu, Y. Zhong, H. Mao, J. Yang, R. Dai, X. Hu, Z. Xing, W. Sheng, L. Tan, Y. Chen, *Chem. Eng. J.* **2022**, *431*, 134235.
[57] J. C. Yu, S. Badgujar, E. D. Jung, V. K. Singh, D. W. Kim, J. Gierschner, E. Lee, Y. S. Kim, S. Cho, M. S. Kwon, M. H. Song, *Adv. Mater.* **2019**, *31*, 1805554.

Manuscript received: June 28, 2022
Accepted manuscript online: August 18, 2022
Version of record online: September 2, 2022